


# Ultrafast Spin Initialization in a Gated InSb Nanowire Quantum Dot

S. Bednarek,<sup>1</sup> J. Pawłowski,<sup>2,\*</sup> M. Górski,<sup>1</sup> and G. Skowron<sup>1</sup>

<sup>1</sup>*Faculty of Physics and Applied Computer Science, AGH University of Science and Technology, Kraków, Poland*

<sup>2</sup>*Department of Theoretical Physics, Faculty of Fundamental Problems of Technology, Wrocław University of Science and Technology, Wybrzeże Wyspiańskiego 27, 50-370 Wrocław, Poland*

 (Received 27 April 2018; revised manuscript received 22 December 2018; published 6 March 2019)

We propose a fast spin-initialization method for a single electron trapped in an electrostatic quantum dot. The dot is created in a nanodevice composed of a catalytically grown indium antimonide (InSb) nanowire and nearby gates to which control voltages are applied. Initially, we insert a single electron of arbitrary spin into the wire. Operations on spin are performed using the Rashba spin-orbit interaction induced by an electric field. First, a single pulse of voltages applied to lateral gates is used to split the electron wave packet into two parts with opposite spin orientations. Next, another voltage pulse applied to the remaining gates rotates the spins of both parts in opposite directions by  $\pi/2$ . In this way, initially opposite-spin parts eventually point in the same direction, along the axis of the quantum wire. We thus set spin in a predefined direction regardless of its initial orientation. This is achieved in time less than 60 ps, without the use of microwaves, photons, or external magnetic fields.

DOI: [10.1103/PhysRevApplied.11.034012](https://doi.org/10.1103/PhysRevApplied.11.034012)

## I. INTRODUCTION

One of the many quantum-bit implementations is based on the spin of an electron or hole trapped in a semiconductor nanodevice [1–3]. Such a device must be built in a way that allows several fundamental operations to be performed, namely, initialization, manipulation, and readout [4,5]. Most of these can be easily carried out in electrostatic quantum dots (QDs), for which confinement potentials are generated in quantum wells [6–10] or wires [11,12], by voltages applied to local gates. They are also realized in self-assembled QDs [13–17], for which confinement is only obtained due to the presence of heterojunctions of different semiconductors. These operations have to be performed sufficiently fast, as a sequence of calculations has to be completed before the decoherence of spin takes place [9].

The most difficult operation to accomplish turns out to be the spin initialization, that is, orienting spin in a chosen direction before any computations are executed. In self-assembled QDs, the spin of a single electron [13–15] or hole [16–18] can be set by using optical transitions to excitonic or trionic (charged-exciton) states. We can proceed in a similar way in nanowire QDs based on  $\text{InAs}_x\text{P}_{1-x}/\text{InP}$  heterojunctions [19]. On the contrary, in electrostatic QDs, optical initialization through trionic states is not possible, since an attractive potential for electrons is repulsive for holes and thus a stable excitonic state cannot be formed.

In such systems, the Pauli blockade is used [9,10]. This method allows us to set the spin of an electron in parallel to spin of another adjacent electron previously trapped in the QD; however, the spin of the former electron is random. It can be set deterministically by using a strong magnetic field and waiting until the electron relaxes to the ground state [10]. Obtained in this way, initialization is not accurate and takes at least a couple of nanoseconds. However, to initialize a qubit to a known state for further operations, a high-fidelity initialization procedure is necessary [20]. Additionally, to perform quantum error correction, certain ancillary qubits must be continuously reinitialized in ultrashort (relative to decoherence) time scales [21]. The main sources of electron-spin decoherence are interactions with the nuclear spin bath. Our nanodevice structure is similar to the one described in the experimental paper [12], which invokes a coherence time of about 34 ns.

Recently, in [22], we have designed a nanodevice based on a planar semiconductor nanostructure, which allows for spin initialization with fidelity over 99%, lasting about 400 ps. This task can be achieved using the electrostatically controlled Rashba spin-orbit interaction (SOI). In this paper, we propose a device capable of achieving similar fidelity an order of magnitude faster in a quantum wire, a nanostructure that is well within current experimental capabilities and much easier to fabricate than a planar nanostructure. This makes quantum wires an ideal starting point for experimental research on spin initialization in solid-state systems.

\*jaroslaw.pawlowski@pwr.edu.pl

## II. NANODEVICE STRUCTURE

For spin initialization, we propose a nanodevice similar to those used in Refs. [12,23], shown in Fig. 1. On a strongly doped silicon substrate, we place a 100-nm-thick layer of  $\text{SiO}_2$ . Next, we lay down seven 200-nm-wide metallic gates,  $U_i$ , separated by gaps of 50 nm each. They serve to shape the confinement potential along the wire. The gates are then covered with a 160-nm-thick layer of  $\text{Si}_3\text{N}_4$  insulator. On top of the insulator, we put a catalytically grown InSb nanowire, 80 nm in diameter and of length  $L$  exceeding  $1.5 \mu\text{m}$ . On both sides of the wire, in parallel, we put two lateral gates,  $U_{\text{left}}$  and  $U_{\text{right}}$ , at a distance of 50 nm from the wire axis. They are used to generate an electric field along the  $y$  axis. Everything is then covered with  $\text{Si}_3\text{N}_4$  up to 400 nm measured from the substrate. Finally, the top surface of  $\text{Si}_3\text{N}_4$  is covered with a top gate  $U_{\text{top}}$ , which, along with the back gate (formed by the strongly doped substrate), is used to create an electric field parallel to the  $z$  direction.

## III. THE MODEL

The operations on the electron are performed within a range of very low energies near to the conduction-band minimum. The initial voltages are applied to the gates and a parabolic approximation of the resulting potential gives rise to an excitation energy of about  $\hbar\omega = 0.2 \text{ meV}$ , significantly lower than the InSb band gap of 230 meV. This makes the single-band effective mass approximation a reasonable choice. Thus, we use this approximation in all subsequent calculations. Now let us discuss the theoretical model of the nanodevice.

First, we assume that the quantum wire confines a single electron. For the InSb effective mass  $m = 0.014 m_e$ , the energy difference between the ground state and the first excited state of quantized electron motion in perpendicular directions to the wire (80 nm in diameter) equals 40 meV, which is 2 orders of magnitude greater than the energies

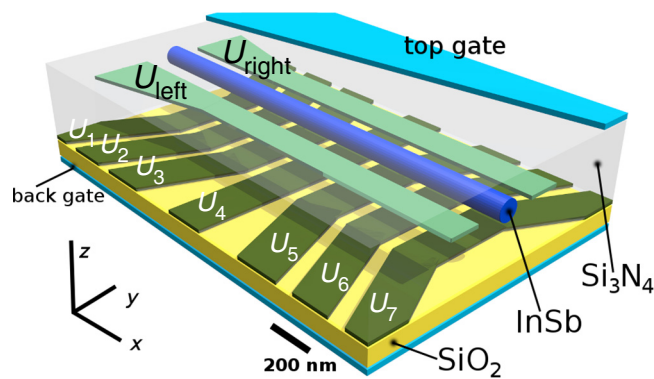


FIG. 1. A schematic view of the proposed nanodevice containing a gated InSb nanowire. The top gate is shown only partially.

of motion encountered in our nanodevice. Thus, we can use a one-dimensional approximation, assuming that the electron always occupies the ground state of lateral motion.

The corresponding Hamiltonian takes the following form:

$$\mathbf{H} = \left[ -\frac{\hbar^2}{2m} \frac{d^2}{dx^2} + V(x) \right] \mathbf{I}_2 + \mathbf{H}_{\text{so}}, \quad (1)$$

where  $V(x)$  is a potential energy of confinement and the last term  $\mathbf{H}_{\text{so}}$  expresses the SOI. The wave function takes the spinor form  $\Psi(x, t) = (\psi_{\uparrow}(x, t), \psi_{\downarrow}(x, t))^T$ .  $\mathbf{I}_2$  denotes a  $2 \times 2$  identity matrix. We assume that the wire is grown along the crystallographic direction [111]; hence the Dresselhaus interaction vanishes [23,24] and we can take into account only the Rashba SOI contribution

$$\mathbf{H}_{\text{so}} = \frac{\alpha_{\text{so}} |e|}{\hbar} (E_z \sigma_y - E_y \sigma_z) \hat{p}_x, \quad (2)$$

with the Pauli matrices  $\sigma_y$  and  $\sigma_z$  and in which the Rashba coefficient for InSb,  $\alpha_{\text{so}} = 523 \text{ \AA}^2$  [24].  $E_y$  and  $E_z$  are the electric-field components within the wire.

If the confinement potential energy has the parabolic form

$$V(x) = \frac{1}{2} m \omega^2 x^2, \quad (3)$$

we can solve for the Hamiltonian eigenfunctions analytically in the momentum representation and then transform them to the position representation. Let us assume that only the  $E_y$  component of  $\mathbf{E}$  is nonzero. The ground-state energy is now doubly degenerated with respect to the spin  $z$  projection. The wave functions in the position representation are Gaussians multiplied by plane waves due to the presence of the SOI. Depending on the spin  $z$  projection, the wave number is either positive  $q$  or negative  $-q$ . The corresponding eigenfunctions take the following form:

$$\begin{aligned} \Psi_{\uparrow}(x) &= \frac{2\beta}{\pi} \begin{pmatrix} 1 \\ 0 \end{pmatrix} e^{-\beta x^2} e^{iqx}, \\ \Psi_{\downarrow}(x) &= \frac{2\beta}{\pi} \begin{pmatrix} 0 \\ 1 \end{pmatrix} e^{-\beta x^2} e^{-iqx}, \end{aligned} \quad (4)$$

where  $\beta = m\omega/2\hbar$  and  $q = m\alpha_{\text{so}}|e|E_y/\hbar^2$ . Although each state's wave function contains a plane-wave factor, the electron remains still as its motion is blocked by the SOI [25]. If we now turn off the electric field abruptly by setting  $E_y = 0$ , the SOI vanishes and the electron starts to move according to its momentum to the left ( $\langle p_x \rangle = -\hbar q$ ) or to the right ( $\langle p_x \rangle = \hbar q$ ), depending on its spin. The SOI introduces an energy correction  $\Delta E = \hbar^2 q^2 / 2m$ , so the maximal electron displacement  $\Delta x$  from the equilibrium

position of the confinement potential [Eq. (3)] approximately obeys the relation  $\Delta E = V(\Delta x)$ , or  $\hbar^2 q^2/2m = (m\omega^2/2)\Delta x^2$ . It follows that

$$\Delta x = \frac{\alpha_{\text{so}}|e|E_y}{\hbar\omega}. \quad (5)$$

Conversely, if the electron relaxes to the ground state with  $E_y = 0$ , abrupt turning on of the electric field will set it in motion, yet in the opposite direction. The effect of spin-dependent motion when the electric field is turned on can be used for the spin readout. The spin orientation of the electron determines its direction of motion (to the left or to the right). Thus, by measuring the electron presence in the left or in the right half of the wire, after the movement takes place, we can infer its spin orientation.

If the initial electron state is not an eigenstate of  $\sigma_z$  (the spin  $z$  projection is not definite), its wave function is a linear combination of both basis states:  $\Psi(x) = c_\uparrow\Psi_\uparrow(x) + c_\downarrow\Psi_\downarrow(x)$ . After the electric field  $E_y$  is changed, both spinor parts start to move along the  $x$  axis in opposite directions and split. If the electric-field pulse is sufficiently strong, it is possible to separate them entirely.

#### IV. THE PRINCIPLES OF SPIN INITIALIZATION

Before we delve deeper into the details of spin initialization, let us first explain the basic principles of this process. Figure 2 shows a simplified model of the nanowire (gray) made of InSb, a material with strong Rashba spin-orbit coupling. Confinement along the wire is created by external-voltage-driven gates, removed from the picture for clarity. We control the voltages applied to these gates to shape the confinement potential, while a few more gates are used to create the electric fields necessary for inducing the Rashba SOI, which is essential for the operation of the device. The initialization scheme consists of two stages.

In the first stage, we insert an electron into the quantum wire and trap it inside the confinement potential [Fig. 2(a)]. This electron can be of arbitrary spin, as the described procedure makes no assumptions about its initial orientation. Next, we apply a rising slope of an electric-field pulse  $E_y$  along the  $y$  axis [Fig. 2(b)]. This field induces the Rashba SOI and makes the electron wave function split into two components of opposite spin, which start traveling in opposite directions. As the components travel further, they slow down and finally halt for an instant [Fig. 2(c)]. At this moment, the electric field  $E_y$  is a maximum and the spin components are somewhat separated but they still overlap. Now, the components start to turn back toward the center of the wire due to the repelling influence of the confinement potential. At this very moment, we apply a falling slope of the electric field  $E_y$  [Fig. 2(d)]. This accelerates the components toward each other and makes them cross unaffected. This acceleration occurs because any change of the electric field  $E_y$  affects the components' motion.

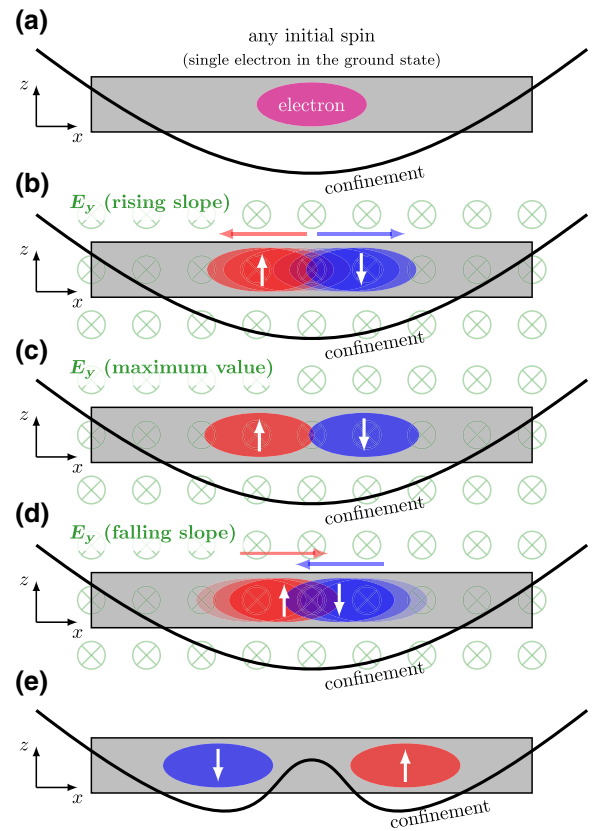


FIG. 2. The first stage of spin initialization. (a) An electron of arbitrary spin orientation is confined within a quantum wire and occupies the ground state. (b) The rising slope of the electric-field pulse  $E_y$  along the  $y$  axis, due to the Rashba SOI, triggers motion of the electron-wave-function spin components in opposite directions, resulting in spin separation. (c) When the spin components are separated the most, the electric field is a maximum. The components, however, still overlap and require stronger separation. (d) The falling slope of the electric-field pulse  $E_y$ , employed when the spin components start turning back, accelerates them even more, making them cross each other and reach positions that are farther apart. (e) The introduction of a potential barrier between the spin components isolates them from their mutual influence and locks their new positions. White arrows along with red or blue colors indicate the spin orientation of each component.

If the electrons were still moving away from each other, the falling slope of  $E_y$  would decelerate them, but since they have already turned back, the falling slope actually accelerates them further. This peculiar behavior has been described in detail in Ref. [25]. Now, after the components have crossed each other, they start to slow down and halt in new positions, separated by a distance that is considerably larger than previously. We need only set a potential barrier between them to lock them in their new positions [Fig. 2(e)]. As the components no longer overlap, this indicates full spin separation. This concludes the first stage of initialization.

Now, the second stage of initialization proceeds, as shown in Fig. 3. We start from the point at which the previous stage finishes. By modifying the voltages applied to the gates forming the electron-confinement potential, we move the potential minima apart slightly, thus setting both spin components in motion in opposite directions [Fig. 3(a)]. At the same time, we apply an electric field  $E_z$  along the  $z$  axis, which induces spin rotations about the  $y$  axis. We must not use the term “spin components” anymore, as they no longer represent spin up and down with respect to the  $z$  axis. From now on, we merely call them wave-function parts. Because the parts move in opposite directions, their spins rotate about the same axis but by opposite angles. After they travel over some distance, they are brought back to their previous locations by the appropriate formation of the confinement potential [Fig. 3(b)]. At this point, we also have to reverse the  $E_z$  direction, because otherwise not only the positions but also the spins

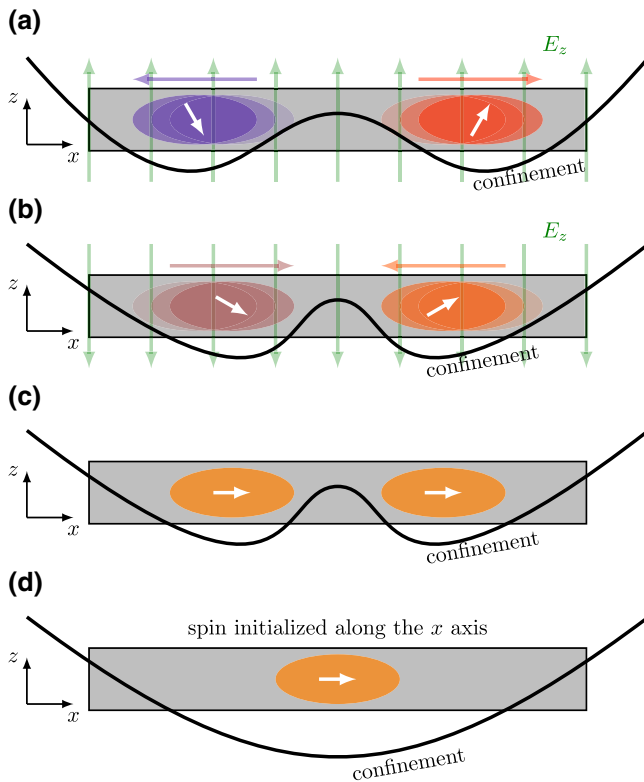


FIG. 3. The second stage of spin initialization. (a) By applying the electric field  $E_z$  along the  $z$  axis and modifying the positions of the confinement potential minima, the spin components’ motion along the wire and the spin rotation about the  $y$  axis are induced. (b) By reverting to the original positions of the minima and reversing the electric field, the spins are further rotated and the wave-function components are brought back to their previous positions. (c) The spins of both former spin components are now oriented in the same direction, effectively ending the initialization procedure. (d) Two wave-function parts can now be brought back together to create a single wave packet.

of both parts would revert to their original orientations, jeopardizing our efforts. Dividing the spin rotation into two small steps—movement forward and movement backward—is advantageous as it prevents the wave-function parts from traveling long distances and allows for simpler control-gate layouts. After the spin rotation, the spins of the wave-function parts are now directed along the  $x$  axis, as shown in Fig. 3(c). Finally, after we turn off the  $E_z$  field, both parts can be brought back and merged to form a single wave packet [Fig. 3(d)]. This concludes the second and last stage of spin initialization.

## V. SIMULATIONS

We perform time-dependent simulations of the nanodevice operation. We use the generalized Poisson equation to solve for the potential  $\phi(\mathbf{r}, t)$  at every time step in a computational box encompassing the entire nanodevice. The obtained potential is used to calculate the potential-energy profile within the quantum wire and along its axis  $V(x, t) = -|e|\phi(x, y_0, z_0, t)$  (where  $y_0$  and  $z_0$  are the coordinates of the wire), as well as the electric field  $\mathbf{E}(\mathbf{r}, t) = -\nabla\phi(\mathbf{r}, t)$ . The time evolution of the electron is obtained by solving the time-dependent Schrödinger equation, starting from the

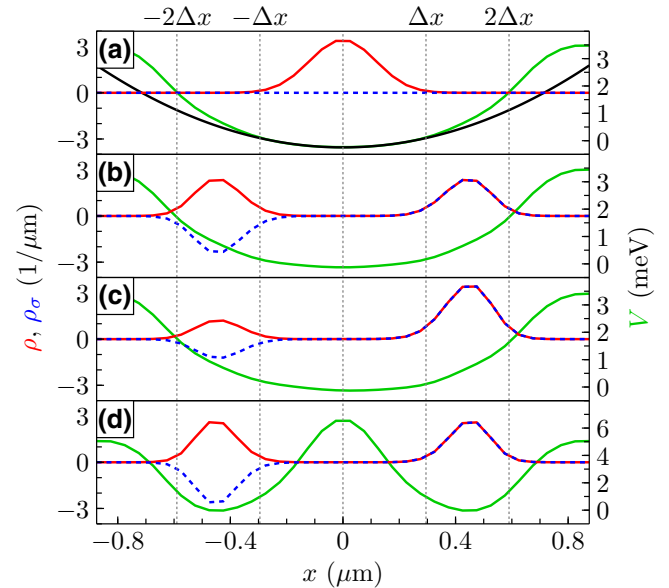


FIG. 4. The electron (red) and spin (blue) densities, together with the electron potential energy (green) along the quantum wire for three selected moments of time: (a) at the beginning, the black line being a parabola fitted near the potential-energy center; (b) after spin separation of an initial state, which is an equally weighted linear combination of  $\Psi_\uparrow$  and  $\Psi_\downarrow$ ; (c) just like (b) but with an initial state that is an exemplary *nonequally* weighted linear combination of  $\Psi_\uparrow$  and  $\Psi_\downarrow$ ; (d) after setting up a potential-energy barrier between wave-packet parts with opposite spin.



electron ground state for the initial potential. A detailed description of the method can be found in Ref. [26].

Initially, the voltages of the top and lateral gates are set to zero:  $U_{\text{top}} = U_{\text{left}} = U_{\text{right}} = 0$ . To the remaining seven lower gates, we apply  $U_{1,\dots,7} = -40$  mV,  $-10$  mV,  $-2.5$  mV,  $0$  mV,  $-2.5$  mV,  $-10$  mV, and  $-40$  mV. These voltages create a confinement potential energy with a nearly parabolic center and high barriers at the borders. The potential-energy profile is shown in Fig. 4(a) as a green line along with a parabolic fit (black line). The red line marks the charge density (i.e., the square of the modulus of the wave function  $\Psi^\dagger(x)\Psi(x)$ ). We assume that, initially, the wave function corresponds to the electron ground state.

Because  $U_{\text{top}} = U_{\text{left}} = U_{\text{right}} = 0$  and the voltages  $U_i$  are relatively small, the electric-field components  $E_y$  and  $E_z$  are nearly zero. This effectively causes vanishing of the SOI. Let us now assume that the spin  $z$  projection is indefinite and that the electron wave function is a linear combination of both spin basis states. To the gates  $U_{\text{left}}$  and  $U_{\text{right}}$ , we apply a single voltage pulse lasting half a period, given by the formulas  $U_{\text{left}}(t) = -U_{\text{sep}} \sin(\omega_{\text{sep}}t)$  and  $U_{\text{right}}(t) = U_{\text{sep}} \sin(\omega_{\text{sep}}t)$ , where  $t \in [0, \pi/\omega_{\text{sep}}]$ , the amplitude  $U_{\text{sep}} = 1.3$  V, and  $\hbar\omega_{\text{sep}} = 0.15$  meV. This pulse generates an electric field parallel to the  $y$  axis and, equivalently the Rashba SOI, which causes spatial separation of the wave function into two parts with opposite spin directions.

Figure 5 shows the results of the electron-state time evolution. The black curve shows a time course of  $U_{\text{left}}(t)$ , the solid red curve the expectation value of the position calculated for the upper spinor part as  $\langle x \rangle_\uparrow = \langle \psi_\uparrow | \hat{x} | \psi_\uparrow \rangle / \langle \psi_\uparrow | \psi_\uparrow \rangle$ , and the dashed red curve  $\langle x \rangle_\downarrow$  calculated in a similar way using the lower spinor part  $\psi_\downarrow$ . Initially, at  $t = 0$ , both  $x_\uparrow$  and  $x_\downarrow$  are identical and correspond to the middle of the wire, where the potential-energy minimum is located. An increasing voltage between  $U_{\text{left}}$  and  $U_{\text{right}}$  induces separation of both wave-packet parts. At  $t = 7$  ps, when the voltage pulse reaches its maximum, the wave-packet parts cease to separate any further and start to move backward. At this moment, the spacing between both parts, calculated from Eq. (5), equals  $2\Delta x = 590$  nm. This agrees only approximately with the more accurate value 505 nm obtained from the simulation shown in Fig. 5 (marked with a cyan arrow). This is so because the Poisson equation solved in the simulations additionally takes into account the interaction of the electron with charge induced on local gates. From now on, the spin-orbit coupling decreases but still accelerates both wave-packet parts, since they bounce off of the potential-energy barriers and move in opposite directions [25]. As a result, the wave-packet energy continues to grow until the voltage pulse returns to zero. For an exactly parabolic potential energy, the spacing between wave-packet parts would be twice as large (and equal to  $4\Delta x$ ), but the actual potential

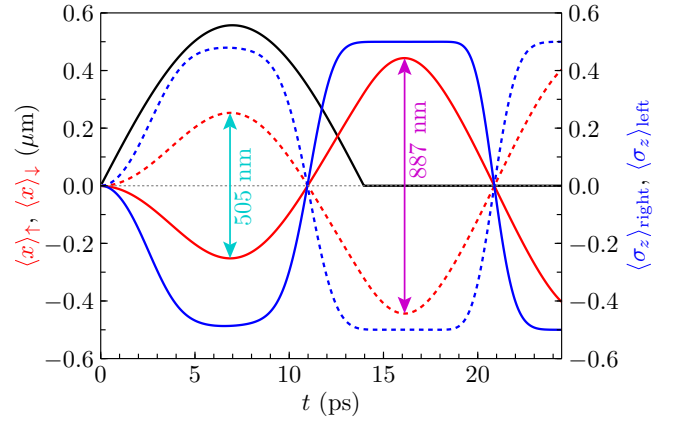


FIG. 5. Time courses in the spin separation stage. The black curve shows the voltage pulse applied to gate  $U_{\text{left}}$ . The red curves (solid and dashed) show the expectation values of the positions of both spin parts of the wave function ( $\langle x \rangle_\uparrow$  and  $\langle x \rangle_\downarrow$ ), while the blue curves show the expectation values of the Pauli  $z$  matrix calculated in the right ( $\langle \sigma_z \rangle_{\text{right}}$ ) and left ( $\langle \sigma_z \rangle_{\text{left}}$ ) halves of the nanodevice.

energy does not satisfy this condition and changes its shape during the wave-packet separation.

Note that the entire process is not resonant and  $\omega_{\text{sep}}$  does not have to be equal to  $\omega$  from Eq. (3). Because the assumed value of  $\omega_{\text{sep}}$  is approximately 20% lower than  $\omega$ , in Fig. 5 the opposite-spin wave packets return to the initial position sooner (at  $t = 11$  ps) than the voltages fall down to zero (at  $t = 14$  ps).

The solid blue curve in Fig. 5 depicts the expectation value of the Pauli  $z$  matrix, calculated in the right half of the quantum wire as (note the limits):

$$\langle \sigma_z \rangle_{\text{right}} = \int_0^{L/2} \Psi^\dagger(x, t) \sigma_z \Psi(x, t) dx. \quad (6)$$

The value of  $\langle \sigma_z \rangle_{\text{left}}$ , calculated in a similar way, is shown in Fig. 5 as a dashed blue line. In the presented simulation, the initial electron state is an equally weighted linear combination of spin states (i.e.,  $c_\uparrow = c_\downarrow = 1/\sqrt{2}$ ); thus at  $t = 15$  ps,  $\langle \sigma_z \rangle_{\text{right}} = 0.5$  and  $\langle \sigma_z \rangle_{\text{left}} = -0.5$ . This indicates a full spatial separation of the spin parts, as shown in Fig. 4(b). If the initial linear combination of spin states is not equally weighted, the final values of  $|\langle \sigma_z \rangle_{\text{right}}|$  and  $|\langle \sigma_z \rangle_{\text{left}}|$  will not be equal. This situation is shown in Fig. 4(c). In the most extreme case, when the spin is oriented upward, i.e.,  $c_\uparrow = 1$  (or downward,  $c_\downarrow = 1$ ), the electron will occupy the right (or left) half of the quantum wire with probability 1. Let us note that this stage of operation can also be used for spin readout. This operation can be performed in  $T_{\text{readout}} = 15$  ps.

Figure 4(b) shows the electron density along the wire (red curve) calculated as  $\rho(x, t) = \Psi^\dagger(x, t)\Psi(x, t) = |\psi_\uparrow(x, t)|^2 + |\psi_\downarrow(x, t)|^2$  and the spin density (blue curve)

as  $\rho_\sigma(x, t) = \Psi^\dagger(x, t)\sigma_z\Psi(x, t) = |\psi_\uparrow(x, t)|^2 - |\psi_\downarrow(x, t)|^2$ . According to these definitions, in the region where the spin is directed upward the curves overlap, which occurs in the right side of the nanodevice, while for spin directed downward they have opposite signs, which occurs in the left side. At the moment when the distance between the wave packets is maximal, we change gate voltages appropriately, creating a potential barrier between them and confining them inside two separate potential valleys. The barrier has to be sufficiently high and the minima sufficiently deep so as to allow independent operations on spin in both valleys. To achieve this, at  $t_1 = 16$  ps we change the gate voltages rapidly to  $U_{1,\dots,7}(t_1) = -60$  mV, 10 mV,  $-10$  mV,  $-100$  mV,  $-10$  mV, 10 mV, and  $-60$  mV. The obtained potential-energy profile as well as the electron and spin densities are plotted in Fig. 4(d). The potential energy has two minima with a barrier between them, separating the wave function spatially into two parts with opposite spin directions.

Now, we proceed to the second stage of the operation, which boils down to a spin rotation about the  $y$  axis. If we turn the spin in the right valley clockwise by  $\pi/2$  and in the left—counterclockwise by the same angle, the spins of both parts become parallel to each other and directed along the  $x$  axis. From the form of the Hamiltonian given in Eq. (1), it follows that the motion along the  $x$  axis induces spin rotation about the  $y$  axis if an electric field  $E_z$  (along the  $z$  axis) is present. We generate it by applying a voltage to the top gate. Now, spin rotation is achieved by setting the electron in an oscillatory motion along the  $x$  direction.

To achieve this, from time  $t_1$  onwards, the voltages applied to gates  $U_2$  and  $U_3$  are modified according to the formulas  $U_2(t) = U_2(t_1) - U_{\text{osc}}\{1 - \cos[\omega_{\text{rot}}(t - t_1)]\}$  and  $U_3(t) = U_3(t_1) + U_{\text{osc}}\{1 - \cos[\omega_{\text{rot}}(t - t_1)]\}$ . Because we want to rotate the spin of both wave-packet parts in opposite directions, to gates  $U_5$  and  $U_6$ , we must apply voltages stimulating motion in the opposite direction:  $U_5(t) = U_3(t)$  and  $U_6(t) = U_2(t)$ . At the same time  $t = t_1$ , we turn on the Rashba SOI, then reverse its sign when the wave-packet parts stop and start to move backward. This is achieved by applying a voltage, phase-shifted by  $\pi/2$ , to the top gate:  $U_{\text{top}}(t) = -U_{\text{rot}} \sin[\omega_{\text{rot}}(t - t_1)]$  [27]. In this simulation stage, the pulse duration equals one single period  $2\pi/\omega_{\text{rot}}$ . The use of a pulse lasting half a period does not produce satisfactory fidelity of spin initialization. The value  $\omega_{\text{rot}}$  does not have to be carefully selected, but it should not be too small, as it affects the duration of operation, and not too large, because with its increase, fidelity drops. In the simulations, we assume a value of  $\hbar\omega_{\text{rot}} = 0.11$  meV. The amplitude  $U_{\text{osc}}$  of the voltages stimulating the wave-packet oscillations does not have to be precisely chosen and we assume  $U_{\text{osc}} = 100$  mV. Also, the exact shape of the pulses is not critical and deviations from the presented sine-like shapes are acceptable. Only the  $U_{\text{rot}}$  amplitude must be tuned to the pulse duration. The

performed simulations indicate that to maintain fidelity at a level of 99% or greater,  $U_{\text{rot}}$  should be selected with an accuracy better than  $\pm 40$  mV.

Figure 6 shows the time evolution of the expectation values of the Pauli  $x$  matrix  $\langle\sigma_x\rangle$  for several initial spin orientations. The courses differ considerably only in the first stage of nanodevice operation, lasting about 7 ps. At  $t = t_1 = 16$  ps, the wave packet is split into two parts, one of which has spin parallel to the  $z$  axis, while the second one has spin antiparallel. At this moment,  $\langle\sigma_x\rangle$  vanishes. In the second stage of simulation, in which the spin parts are rotated, the courses overlap regardless of the initial spin orientations and all reach a value close to unity at the same time:  $t = 60$  ps. The final fidelity of the spin initialization is of the order of 99.3%.

After the entire procedure, the spin becomes oriented along the  $x$  direction. However, if we want to further change its orientation, this can be done using another voltage pulse. Voltages applied to the lateral gates can generate the SOI, which induces spin rotation about the  $z$  axis. On the other hand, a voltage applied to the top gate allows for rotations about the  $y$  axis.

The second pulse, visible in Fig. 6 and lasting about 45 ps, results in a spin rotation by  $90^\circ$ . Such an operation is performed by the Hadamard gate and in our case it takes  $T_{\text{Hadamard}} = 45$  ps. The NOT gate requires a rotation by  $180^\circ$ ; thus it requires  $T_{\text{NOT}} = 90$  ps. During the second stage of the presented initialization scheme, we rotate the spin in the right potential valley clockwise and in the left potential valley, counterclockwise. If the spin is rotated by  $180^\circ$  only in the left valley, leaving the right one unchanged, which can be achieved by modulating voltages  $U_2$  and  $U_3$  and fixing voltages  $U_5$  and  $U_6$ , the spin of the electron will be reversed if it occupies the left valley or will remain untouched if it occupies the right one. This

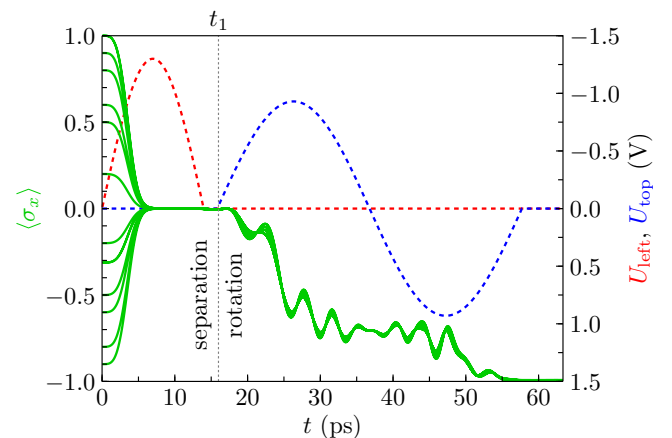


FIG. 6. The time courses of the expectation values of the Pauli  $x$  matrix, namely  $\langle\sigma_x\rangle$ , for various initial spin orientations (green). The red dashed curve shows the separating voltage pulse, while the blue dashed curve shows the pulse responsible for the SOI, used for spin rotations in both parts of the device.

outcome is equivalent to the controlled negation (CNOT) two-qubit gate if we assume that the first qubit is a spin qubit while the second is a charge qubit, defined as the presence of an electron in the left or right potential valley. The operation time of this gate is  $T_{\text{CNOT}} = 90$  ps.

## VI. CONCLUSION

We propose a nanodevice designed to set the spin of a single electron in a desired direction. After two voltage pulses lasting less than 60 ps in total, the spin is set in parallel to the  $x$  axis. The outcome does not depend on the initial spin orientations and is obtained without the use of any external fields, microwaves, or photons. The goal is achieved all-electrical means, with voltages applied to the local gates. The proposed nanodevice can also be used to perform other necessary quantum operations: readout, the Hadamard gate, the NOT gate, and the CNOT gate, in times 15 ps, 45 ps, 90 ps, and 90 ps, respectively. Compared to the coherence time of about 34 ns, these estimated operation times look very promising.

In the performed simulations, the nanodevice is modeled upon other similar nanostructures described in experimental papers, which assures its experimental feasibility. We use real material parameters such as the InSb electron effective mass or distinct dielectric constants of the nanowire and the surrounding insulator. The assumed electric pulse durations are short yet experimentally achievable, while their amplitudes are low enough to ensure adiabaticity of the entire process. The estimated operation times are extracted directly from the time courses in Fig. 6. They are achievable in practice but shortening them any further might prove difficult.

## ACKNOWLEDGMENTS

This work has been supported by the National Science Centre (NSC), Poland, under Grant No. UMO-2014/13/B/ST3/04526. J.P. has been supported by the National Science Centre, under Grant No. 2016/20/S/ST3/00141. This work was also partially supported by the Faculty of Physics and Applied Computer Science AGH UST Dean Grants No. 15.11.220.717/24 and No. 15.11.220.717/30 for Ph.D. students and young researchers through a subsidy from the Ministry of Science and Higher Education.

- 
- [1] Daniel Loss and David P. DiVincenzo, Quantum computation with quantum dots, *Phys. Rev. A* **57**, 120 (1998).
  - [2] N. Samarth, D. D. Awschalom, and D. Loss, eds., *Semiconductor Spintronics and Quantum Computation* (Springer-Verlag, Berlin Heidelberg, 2002).
  - [3] Christoph Kloeffel and Daniel Loss, Prospects for spin-based quantum computing in quantum dots, *Annu. Rev. Condens. Matter Phys.* **4**, 51 (2013).

- [4] David P. DiVincenzo, The physical implementation of quantum computation, *Fortschritte Phys.* **48**, 771 (2000).
- [5] Michael A. Nielsen and Isaac L. Chuang, *Quantum Computation and Quantum Information: 10th Anniversary Edition* (Cambridge University Press, Cambridge, UK, 2010).
- [6] J. M. Elzerman, R. Hanson, L. H. Van Beveren, B. Witkamp, L. M. K. Vandersypen, and Leo P. Kouwenhoven, Single-shot read-out of an individual electron spin in a quantum dot, *Nature* **430**, 431 (2004).
- [7] J. R. Petta, A. C. Johnson, J. M. Taylor, E. A. Laird, A. Yacoby, M. D. Lukin, C. M. Marcus, M. P. Hanson, and A. C. Gossard, Coherent manipulation of coupled electron spins in semiconductor quantum dots, *Science* **309**, 2180 (2005).
- [8] K. C. Nowack, F. H. L. Koppens, Yu. V. Nazarov, and L. M. K. Vandersypen, Coherent control of a single electron spin with electric fields, *Science* **318**, 1430 (2007).
- [9] R. Hanson, L. P. Kouwenhoven, J. R. Petta, S. Tarucha, and L. M. K. Vandersypen, Spins in few-electron quantum dots, *Rev. Mod. Phys.* **79**, 1217 (2007).
- [10] K. C. Nowack, M. Shafiei, M. Laforest, G. E. D. K. Prawiroatmodjo, L. R. Schreiber, C. Reichl, W. Wegscheider, and L. M. K. Vandersypen, Single-shot correlations and two-qubit gate of solid-state spins, *Science* **333**, 1269 (2011).
- [11] S. Nadj-Perge, S. M. Frolov, E. P. A. M. Bakkers, and Leo P. Kouwenhoven, Spin-orbit qubit in a semiconductor nanowire, *Nature* **468**, 1084 (2010).
- [12] J. W. G. van den Berg, S. Nadj-Perge, V. S. Pribiag, S. R. Plissard, E. P. A. M. Bakkers, S. M. Frolov, and L. P. Kouwenhoven, Fast Spin-Orbit Qubit in an Indium Antimonide Nanowire, *Phys. Rev. Lett.* **110**, 066806 (2013).
- [13] Mete Atatüre, Jan Dreiser, Antonio Badolato, Alexander Högele, Khaled Karrai, and Atac Imamoglu, Quantum-dot spin-state preparation with near-unity fidelity, *Science* **312**, 551 (2006).
- [14] Xiaodong Xu, Yanwen Wu, Bo Sun, Qiong Huang, Jun Cheng, D. G. Steel, A. S. Bracker, D. Gammon, C. Emary, and L. J. Sham, Fast Spin State Initialization in a Singly Charged InAs-GaAs Quantum Dot by Optical Cooling, *Phys. Rev. Lett.* **99**, 097401 (2007).
- [15] David Press, Thaddeus D. Ladd, Bingyang Zhang, and Yoshihisa Yamamoto, Complete quantum control of a single quantum dot spin using ultrafast optical pulses, *Nature* **456**, 218 (2008).
- [16] Brian D. Gerardot, Daniel Brunner, Paul A. Dalgarno, Patrik Öhberg, Stefan Seidl, Martin Kroner, Khaled Karrai, Nick G. Stoltz, Pierre M. Petroff, and Richard J. Warburton, Optical pumping of a single hole spin in a quantum dot, *Nature* **451**, 441 (2008).
- [17] Jonathan D. Mar, Jeremy J. Baumberg, Xiulai Xu, Andrew C. Irvine, and David A. Williams, Ultrafast high-fidelity initialization of a quantum-dot spin qubit without magnetic fields, *Phys. Rev. B* **90**, 241303 (2014).
- [18] A. J. Brash, L. M. P. P. Martins, F. Liu, J. H. Quilter, A. J. Ramsay, M. S. Skolnick, and A. M. Fox, High-fidelity initialization of long-lived quantum dot hole spin qubits by

- reduced fine-structure splitting, *Phys. Rev. B* **92**, 121301 (2015).
- [19] Konstantinos G. Lagoudakis, Peter L. McMahon, Kevin A. Fischer, Shruti Puri, Kai Müller, Dan Dalacu, Philip J. Poole, Michael E. Reimer, Val Zwiller, Yoshihisa Yamamoto, and Jelena Vučković, Initialization of a spin qubit in a site-controlled nanowire quantum dot, *New J. Phys.* **18**, 053024 (2016).
- [20] A. Noiri, T. Nakajima, J. Yoneda, M. R. Delbecq, P. Stano, T. Otsuka, K. Takeda, S. Amaha, G. Allison, K. Kawasaki, A. Ludwig, A. D. Wieck, D. Loss, and S. Tarucha, A fast quantum interface between spin qubits of different codes, arXiv:1804.04764 [cond-mat.mes-hall] (2018).
- [21] John Preskill, Reliable quantum computers, *Proc. R. Soc. London A: Math. Phys. Eng. Sci.* **454**, 385 (1998).
- [22] S. Bednarek, J. Pawowski, M. Górski, and G. Skowron, All-electric single electron spin initialization, *New J. Phys.* **19**, 123006 (2017).
- [23] S. Nadj-Perge, V. S. Pribiag, J. W. G. van den Berg, K. Zuo, S. R. Plissard, E. P. A. M. Bakkers, S. M. Frolov, and L. P. Kouwenhoven, Spectroscopy of Spin-Orbit Quantum Bits in Indium Antimonide Nanowires, *Phys. Rev. Lett.* **108**, 166801 (2012).
- [24] Roland Winkler, *Spin-Orbit Coupling Effects in Two-Dimensional Electron and Hole Systems* (Springer-Verlag, Berlin Heidelberg, 2003).
- [25] J. Pawowski, M. Górski, G. Skowron, and S. Bednarek, Generation of Schrödinger cat type states in a planar semiconductor heterostructure, *Phys. Rev. B* **96**, 115308 (2017).
- [26] S. Bednarek, B. Szafran, R. J. Dudek, and K. Lis, Induced Quantum Dots and Wires: Electron Storage and Delivery, *Phys. Rev. Lett.* **100**, 126805 (2008).
- [27] J. Pawowski, P. Szumniak, and S. Bednarek, Electron spin rotations induced by oscillating Rashba interaction in a quantum wire, *Phys. Rev. B* **93**, 045309 (2016).